Article

Green Synthesis, Characterization and Antibacterial Activity of Gold and Copper Nanoparticles from Lannea discolor (Sond.) Engl

Unarine Rambau , Nndivhaleni Anox Masevhe * , Nneka Augustina Akwu , Amidou Samie

Posted Date: 1 December 2023

doi: 10.20944/preprints202312.0090.v1

Keywords: copper nanoparticles; gold nanoflowers; green nanoparticle synthesis; Lannea discolor; plant extracts

Article

Green Synthesis, Characterization and Antibacterial Activity of Gold and Copper Nanoparticles from *Lannea discolor* (Sond.) Engl

Unarine Rambau [1], Ndivhaleni Anox Masevhe [1,*], Nneka Augustina Akwu [2,3] and Amidou Samie [4]

[1] Department of Biological Sciences, Faculty of Science, Engineering and Agriculture, University of Venda, Private Bag X5050, Thohoyandou 0950, South Africa; unarambau@gmail.com (U.R); Nndivhaleni.Masevhe@univen.ac.za (N.A.M)
[2] Indigenous Knowledge Systems Centre, Faculty of Natural and Agricultural Sciences, North-West University, Private Bag X2046, Mmabatho, 2790, South Africa; nneka.akwu@yahoo.com (N.A.A)
[3] Preclinical Drug Development Platform, Faculty of Health Sciences, North-West University, Private Bag X6001, Potchefstroom, 2520, South Africa; nneka.akwu@yahoo.com (N.A.A)
[4] Department of Biochemistry and Microbiology, Faculty of Science, Engineering and Agriculture, University of Venda, Private Bag X5050, Thohoyandou 0950, South Africa. (A.S)
* Correspondence: Nndivhaleni.Masevhe@univen.ac.za (N.A.M)

Abstract: Green synthesis using plant extracts has emerged as an eco-friendly, clean, and viable strategy alternative to chemical and physical approaches. The leaf, stem, and root extracts of *Lannea discolor* was utilized as a reducing and stabilizing agent in the synthesis of gold (AuNPs) and copper (CuNPs) nanoparticles. The formation of AuNPs and CuNPs confirmed by their color change, was characterised by UV–Vis Spectroscopy (UV- Vis), Scanning electron microscopy analysis and energy dispersive x-ray (SEM-EDX), Transmission Electron Microscopy (TEM), and Fourier Transform Infrared Spectroscopy (FTIR), coupled with minimum concentration inhibitory (MIC) antibacterial assays. AuNFs, NPs and CuNPs peaked at wavelengths in the ranges of 316, 544 and 564 nm respectively. TEM showed unexpected nanoflowers (30 – 97 nm) in the leaf extracts and spherical NPs (10 -33 nm; 9.3 – 37.5) from stem and root extracts, while spherical CuNPs (20 – 104 nm), were observed from all the extracts. EDX was able to confirm the presence of metal salts and FTIR revealed stable capping agents. AuNPs and NFs from *L. discolor* extracts showed appreciable antibacterial activity against *Staphylococcus aureus*, *Escherichia coli*, *Pseudomonas aeruginosa*, *Klebsiella pneumoniae* and *Bacillus subtilis*, when compared to the plant extracts, while none was observed from the CuNPs. These AuNPs and CuNPs are particularly appealing in a variety of applications in the biomedical as well as conductivity manufacturing, due to their shapes and sizes and economical and environmentally friendly production.

Keywords: copper nanoparticles; gold nanoflowers; green nanoparticle synthesis; *Lannea discolor*; plant extracts

1. Introduction

Nanotechnology, a globally active research discipline, is rapidly progressing, with nanoparticles being a topic of interest since the 1970s [1]. Nanoparticles (NPs) are microscopic particles with at least one dimension less than 100 nm and can be categorised into different types according to morphology, size, physicochemical properties, and the type of precursor from which they are synthesised [2]. Metal nanoparticles (NPs) are created from metal precursors like gold and copper using synthetic or chemical methods, which may use environmentally unfriendly reducing agents [3]. This has resulted in scientists turning to safer methods of synthesis, by employing biological reductants such as bacterial, fungal and plant material to curb any possible negative effects from nanosynthesis [4]. Gold

 doi:10.20944/preprints202312.0090.v1

nanoparticles (AuNPs) are used in various fields such as gene therapy, protein delivery, cancer diagnosis, photodermal and photodynamic therapy, delivery of antitumor agents, DNA detection and catalysis [5]. Ancient Indian healers used them for asthma and arthritis, later, Romans used them for cathedral glassware decoration. Recently, they functioned as photocatalytic air purifiers, gaining significant therapeutic applications [6]. AuNPs are compatible with living tissue, producing no toxic or immunological response, and have been used as nanocarriers due to their small sizes for anti-inflammatory drugs, improving stability and adsorption efficiencies [7,8]. Plant extracts have gained attention as reducing agents for AuNP synthesis due to their low toxicity, eco-friendliness, and simplicity of production [4,9]. Various plants such as *Anacardium occidentale* [10], *Spondias dulcis* [11], and *Pistacia chinensis* [12], have been reported to be effective in reducing gold ions into differently shaped and sized nanoparticles. Nanotechnology has enabled the development of modern techniques for nano-scale copper generation over the past decade [13]. CuNPs are gaining attention due to their ease of availability and economic feasibility, unlike other noble metals that are similar. They are widely utilized in cancer imaging due to their efficient light-to-heat transformation under near-infrared laser irradiation [13]. Other uses include enhancing heat transfer liquids, photonic devices, sensors and electrochemical devices [14, 15]. CuNPs, with their unique properties, have gained significant applications in various industries such as cosmetology, agriculture, food, textiles, and construction [16,17]. In several studies, CuNPs providing higher environmental mobility were synthesized using various plant extracts including *Cissus vitiginea [17] Zingiber officinalis* and *Curcuma longa* [18] *Brassica oleracea* [19], *Hyptis suaveolens* (L.) [20]. *Lannea discolor* from family Anacardiaceae is a deciduous tree that usually grows up to 15 m on rocky slopes, or on sandy soil. The leaves are discolorous, having a green colored adaxial surface and a grey dense trichome layer on the abaxial surface. Its traditional uses include treatment for diarrhoea, stomach complains, and an array of infections [21]. The pharmacological activities of the plant are purported to be the result of various secondary metabolites such as phenolic flavonoids, alkaloids [22]. Given that CuNPs are a stable substitute for gold, they may serve as low-cost replacement for unattainable precious metals. Conclusively, all NPs were characterized by UV–Vis spectrometry, FT-IR spectroscopy, SEM–EDX and TEM to investigate the optical, morphology and elemental composition as well as the antibacterial activities of nanoparticles, respectively.

2. Results and discussion

2.1. Visual and UV-Vis Spectroscopic Analysis

This study is a simple and sustainable method for synthesizing AuNPs and CuNPs by mixing AuCl4 and CuSO4 solutions with the methanol, acetone and water extracts of *Lannea discolor*. Following incubation of AuCl4 and $CuSO_4$ solutions with extracts, solutions went from dark yellow to greyish for the leaves (Figure 1A, C), and intense violet for the stem and root was observed (Figure 1B, D). The extracts when exposed $CuSO_4$ changed from their usual color to more intensified burnt orange for the leaves (Figure 1E, G) and a brown to a darker brown for the stem and root (Figure 1H).

Preprints (www.preprints.org) | NOT PEER-REVIEWED | Posted: 1 December 2023 doi:10.20944/preprints202312.0090.v1

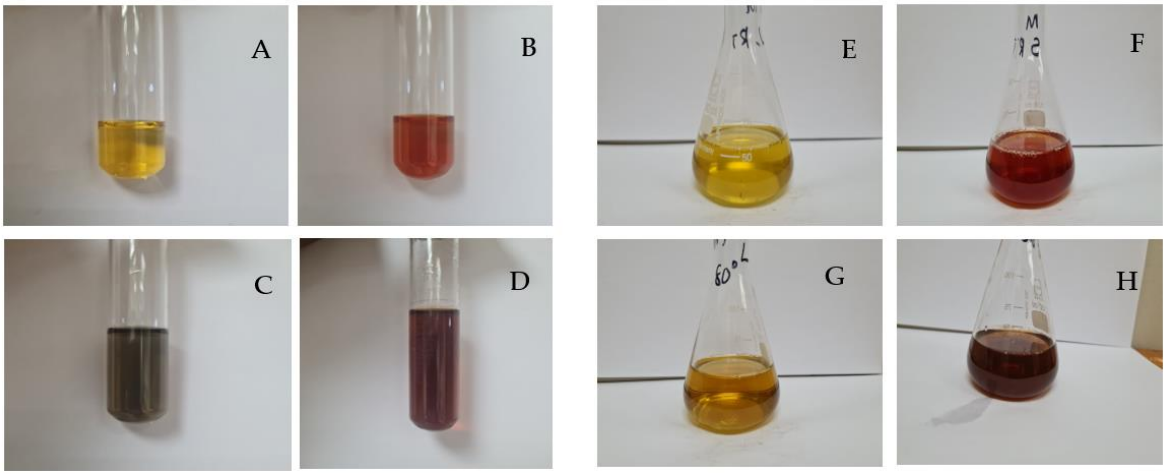

Figure 1. Visual representation of *Lannea discolor* extracts before NP synthesis (A) leaf (B) stem and root (C) AuNPs from leaves (D) AuNPs from stem and root bark. (E) and (F) are solutions before CuNPs synthesis. CuNPs leaf (G) and stem, root (H) after synthesis.

UV–Vis representative absorption spectra for the AuNPs and CuNPs are shown in Figure 2A - B. The absorption peak for the AuNPs from stem and roots extracts, had a maximal absorption at 544 nm, while the leaf extracts NPs solutions peaked at 316 nm. Similar results were observed of the latter, in other studies [23-24]. As much as UV-vis characteristic wavelength of AuNPs has been used to validate the synthesis of NPs, certain peaks may also be attributed to their size and shape, instead of their abundance. The change in color of the NPs solution to grey due to Oswald ripening is a well-understood phenomenon [25]. Similarly, the two-pointed peaks observed in the NPs from the leaf extracts; indicate a different morphology when compared to the stem and roots. Studies show that spherical AuNPs appear red; but visualise blue or grey when they form NFs [26,27].

The CuNPs displayed an absorption peak at ranges of 556 – 564 nm for leaves and 540 -546 nm for stems and roots. As Figures 2A and B show, the increase in the temperature did not significantly reduce or increase the adsorption and synthesis of CuNPs. It is reported in literature, the surface plasmon resonance band of CuNPs provides absorption from 500 to 600 nm [28]. Therefore, CuNPs peaks acquired confirm their formation.

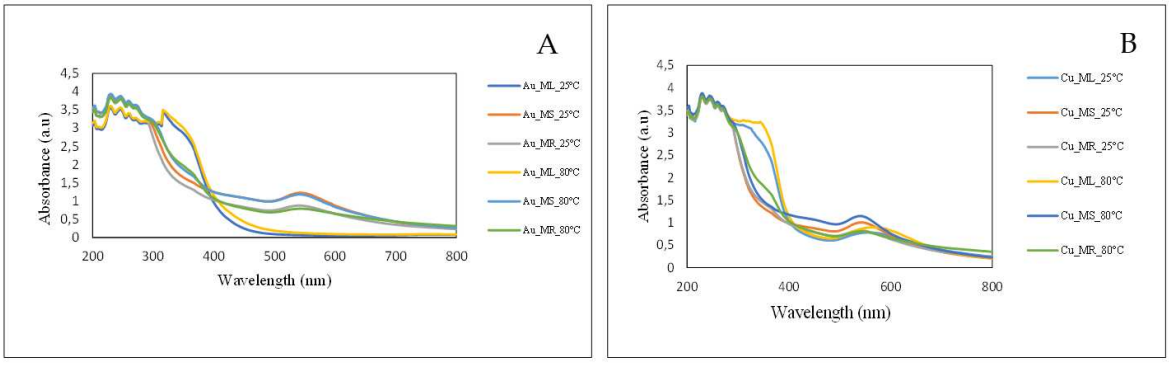

Figure 2. UV-vis spectra of SPR bands representing *Lannea discolor* (A) AuNPs/NFs and (B) CuNPs synthesised at 25 °C and 80 °C.

2.2. Morphology of synthesised nanoparticles using Scanning electron microscopy and Energy dispersive X-ray Analysis

SEM analysis shows in Figure 3A, aggregated AuNPs that were present from all leaf extracts, evidently confirming the influence of the leaf extracts in the morphology observed. Fluorescence emission from is observed in Figure 3B inset. Under the light irradiation, AuNPs emit fluorescence,

Preprints (www.preprints.org) | NOT PEER-REVIEWED | Posted: 1 December 2023 doi:10.20944/preprints202312.0090.v1

a characteristic suggested to confer phototherapy potential and showing the possible optical properties of the AuNPs [29].

CuNPs were found to be spherical in shape (Figure 4A) and aggregated, which is a result of static tension [30]. Furthermore, there is unexpected sintering observed in Figure 4B after exposure to heat. Sintering involves the joining together of nanoparticles into a solid mass, due to temperature less than 250° C, pressure, and leftover alcohols during evaporation [31]. As such, during both synthesis and drying, the CuNPs undergo sintering, and the well-connected features are observed in Figure 4B. Sintering techniques have been standardised to produce chemically synthesised CuNPs for copper inks used in conductivity [31,32], yet no work has been reported employed sintering temperature as low as 60 ◦C for CuNPs from *Lannea discolor* extracts. Literature reports that the optical and electronic properties of NPs depend on morphology [32,33], rendering CuNPs as potentials in these types of applications.

The EDX measurements unambiguously confirmed the presence of metallic Au. The EDX profile shows a strong Au signal along with C, O Al, K, and Ca peaks, from the biomolecules on the surface of the AuNPs (Figure 3C, D). These elements may also be present due to the elemental composition of the extracts, from which the AuNPs were not completely purified [34]. The grid, on which the samples were examined, is what causes the presence of Cu. Thus, all measurement techniques confirmed the presence of AuNPs and NFs. Likewise, the EDX profile of the CuNPs shows strong elemental signals of copper, confirming the presence of CuNPs, as shown in Figure 4C - D. The weight percentages of different elements in the CuNPs were below 10 %, as shown in Figure 4C - D. The remaining Wt % were carbon and oxygen present in organic molecules, which act as capping molecules surrounding the nanoparticles as well as the tape used to mount the CuNPs [35].

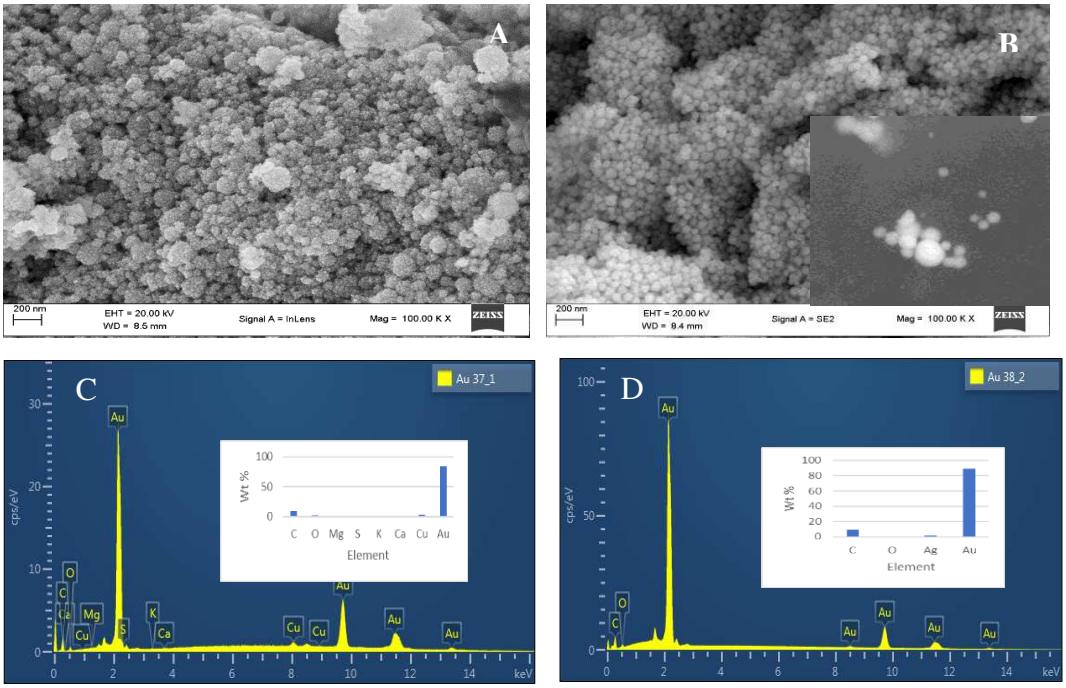

Figure 3. SEM images of (A) AuNFs and (B) AuNPs of *L. discolor* and, (C) and (D) EDX spectra. Inset of (B) image of fluorescence emission from AuNPs. Insets of (C) and (D) contain graphs of abundance of Au.

Preprints (www.preprints.org) | NOT PEER-REVIEWED | Posted: 1 December 2023 doi:10.20944/preprints202312.0090.v1

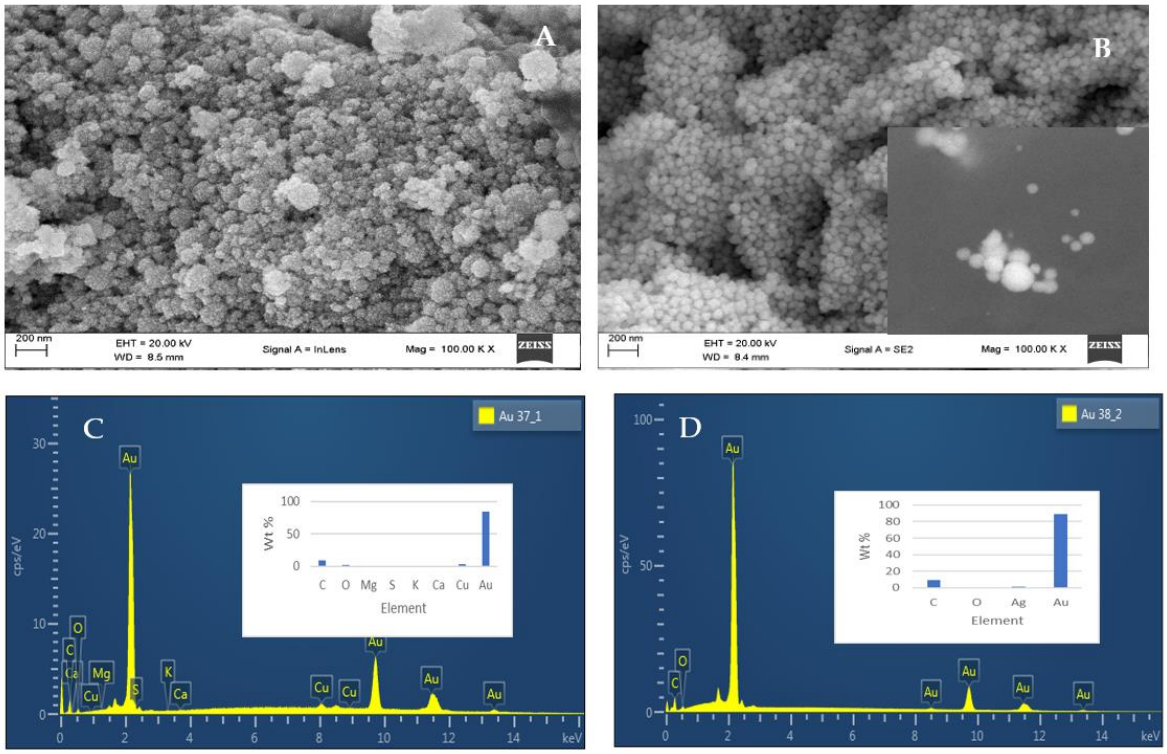

Figure 4. Representative SEM images and EDX spectra of CuNPs from *Lannea discolor*. (A) nanoparticles synthesised at 25° C (B) arrows showing sintering. C and D show EDX spectra and abundance of Cu.

2.3. TEM, Particle Size and Zeta Potential Analysis

TEM images showed NPs with protruding petal-like features, which are confirmed to be NFs [36]. As observed in Figure 5A, the particles are spherical dots with an average diameter ±10 nm. An in-depth morphological analysis suggests that the formation of AuNFs occurs by initial formation of NPs, followed by rapid anisotropic growth, then assembly into a flower shape by secondary reduction at their interface [36]. The rapid color change from yellow to grey without intermediate colours supports this theory of their progression [36]. Thus, we proposed the formation mechanism to be aggregation-based growth, as illustrated in Figure 6**.** Their 3-dimensional, gives AuNFs better suspension stability and a greater surface area than spherical AuNPs [37,38]. Also, significant enhancement of the local electrostatic fields and "petals" are advantageous in catalytic reactions, drug delivery and nuclear medicine [38]. The size of the NFs from *L. discolor* varies from 30 to 97 nm with an average size of 67 nm. Similar sizes were also previously reported by Borah *et al* using *Syzygium cumini* [39]. Onmaz *et al* reported sizes <100 nm NFs using *Helichrysum italicum* [40]. Other studies suggest that tannin-based polymers enhance reduction [41], explaining the unexpected formation of NFs from *L discolor*. NFs have a potential in developing biosensors, such that, through surface modification, their interactions to biomolecules of interest can be detected by a color change [41]. Familiar examples of NPs used in sensing is the home pregnancy test based on detection of the hormone pregnancy (β-HCG hormone) [42]. In other studies, the grey suspension of AuNPs was obtained by chemical synthesis, where trisodium citrate and water-soluble polymer were added to HAuCl4 [43,44]. To move to greener synthesis of NFs, using *L. discolor* leaves may prove to be less tedious and more environmentally friendly. Under the given conditions**,** spherical AuNPs were formed from stem and root extracts ranging at 10 – 33 and 9.3 –37.5 nm respectively (Figure 5B), with lower sizes (Figure 5D), than those obtained in the leaf samples. Shabestariana *et al* acquired spherical AuNPs with an average size of 20.83, from *Rhuscoriaria* L. (*Sumac*), confirming that significant molecules in the extracts act as ligands which control NPs growth [45,46]. Similarly, Donga *et al* reported even smaller sized NPs from *Mangifera indica* ranging at 12.33 – 24.05 nm [47]. Comparably,

Preprints (www.preprints.org) | NOT PEER-REVIEWED | Posted: 1 December 2023 doi:10.20944/preprints202312.0090.v1

Pechyen *et al* reported similar sized spherical AuNPs from *Spondias dulcis* [11]. Figure 5B insets show a triangular, and hexagonal NPs which have been reported by Song *et al* to be caused by low concentration of extracts [48]. However, the effect on the size and shape of AuNPs in the present study may be in response to the plant part and solvent used in extraction, indicating the uniqueness of the phytochemicals in the extracts, and their specific requirements for higher temperatures to initiate the reduction process and produce other morphologies [48].

Figure 7A shows the TEM images of spherical CuNPs with particle size in the range 20 - 104 nm (Figure 7B). In both Figure 7A and inset, NPs are similarly sintered as observed in section 2.2. Authors suggest their large sizes may be more to do with the ability of the present biomolecules to reduce the $CuSO_4$ and their concentration.

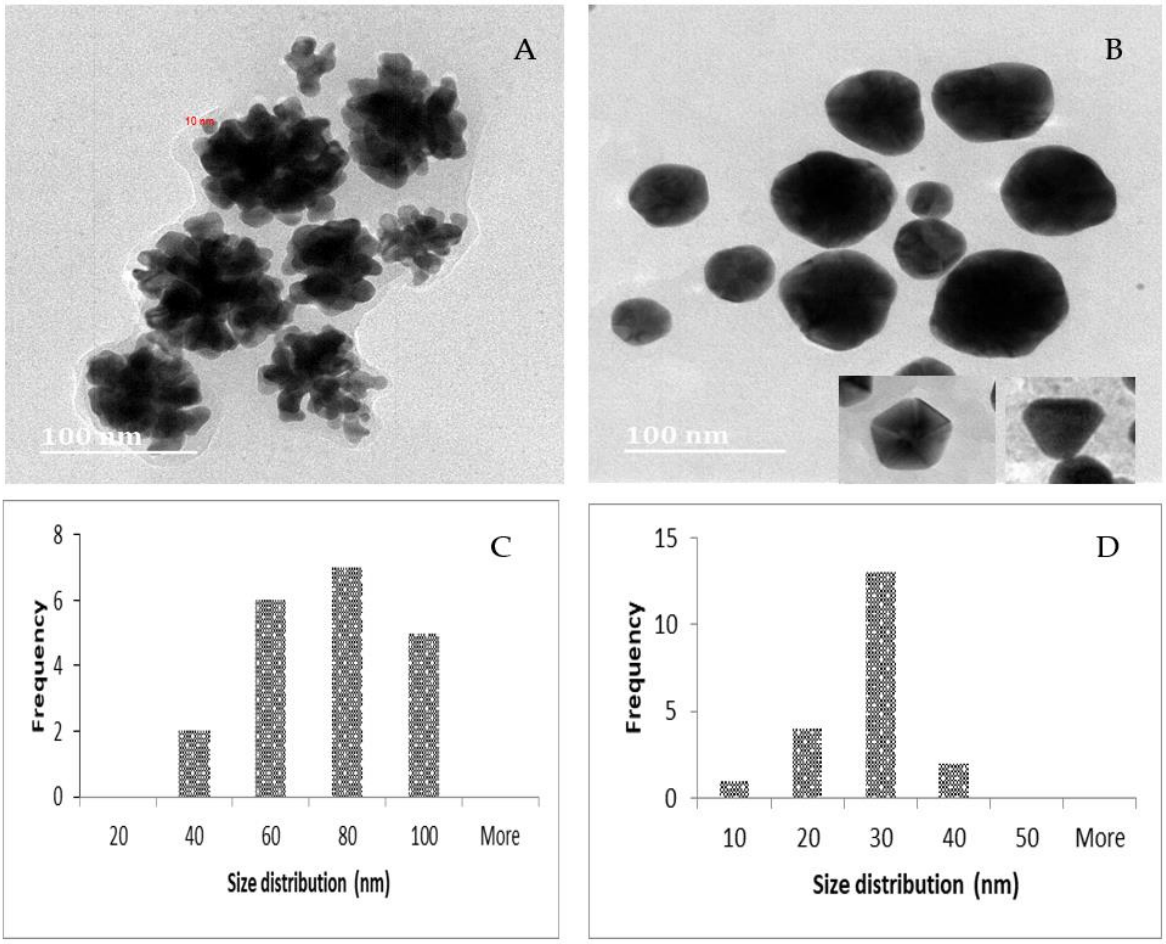

Figure 5. Representative TEM images of the AuNFs (A) from leaves and NPs (B) from stem and root of *L discolor*. Insets in showing triangular and hexagonal NPs. Histograms show size distribution of AuNFs (C) and AuNPs (D).

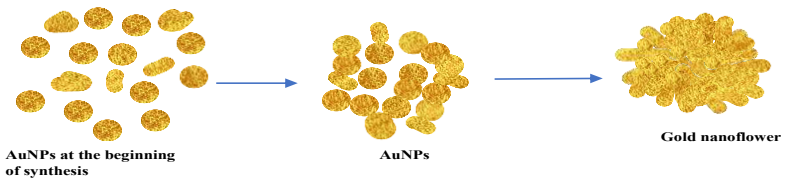

Figure 6. Schematic diagram showing proposed growth mechanism of AuNFs from *Lannea discolor* leaves.

Preprints (www.preprints.org) | NOT PEER-REVIEWED | Posted: 1 December 2023 doi:10.20944/preprints202312.0090.v1

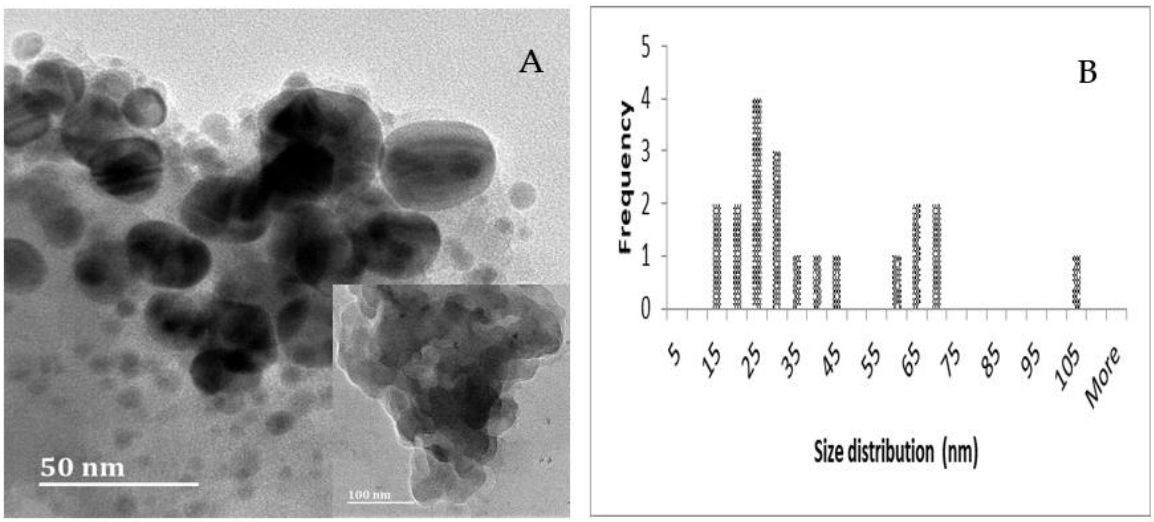

Figure 7. (A) CuNPs and (B) size distribution thereof. Inset showing TEM image of sintering in NPs exposed to high temperatures.

AuNCs and NPs are soluble in water, suggesting high solubility in biofluids and potential as injectables [49]. The corresponding adsorption of these NPs in the body may be improved by their stability, that is measured as zeta potential. In addition, the absolute values of zeta potentials for AuNCs were -14.6, -8.3, -10.8 and - 6.39 mV, indicating their stability, which is due to the larger electrostatic repulsion [2,50]. CuNPs had a stability range of -43.3 to -13.4 mV. Zeta potential greater than 30 mV or less than −30 mV is indicative of stable dispersions of NPs in solutions [50].

2.4. FTIR Analysis

FT-IR measurements of the NPs were carried out to identify the major functional groups of phytochemicals present in *L. discolor* extract. The typical FT-IR spectra of AuNPs and CuNPs synthesized in the presence of *L. discolor* extracts are shown in Figure 8. Bands at 2780, 2873,2816, 3015, 3255, 3272,3299, and 3313 cm $^{-1}$ are due to N–H stretching of both amines and amides and/or to O–H stretching of alcohols, phenols, or carboxylic acids. The aromatic stretches (C-H) observed at peaks 1894, 1935, 1938, 1954, 1973, 1994 cm $^{-1}$ in both the AuNPs and CuNPs may be amongst the main capping agents. The binding characteristics of amino groups in the samples could be the cause of the produced CuNPs' aggregation, which resulted in the sintering [51,52].

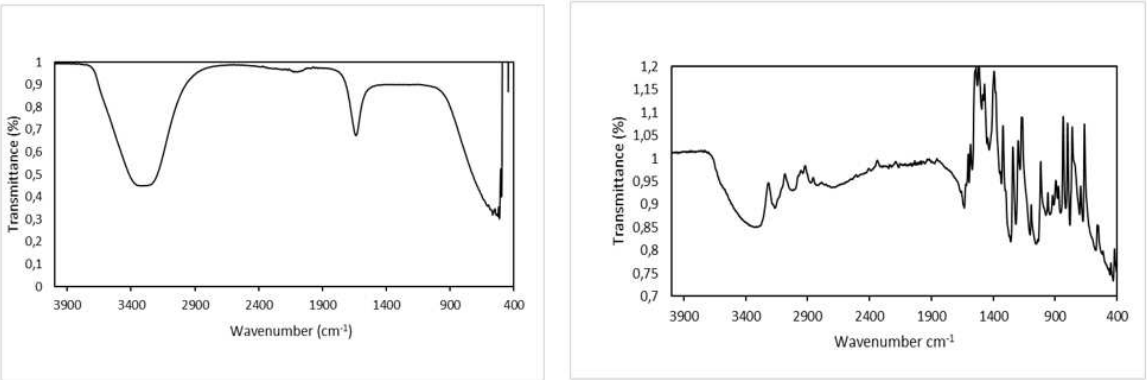

Figure 8. FTIR spectrum of AuNPs (A) and CuNPs (B) from *Lannea discolor*.

2.5. Antibacterial Activity of AuNPs and CuNPs

Preprints (www.preprints.org) | NOT PEER-REVIEWED | Posted: 1 December 2023 doi:10.20944/preprints202312.0090.v1

In addition to previously mentioned applications, NPs may be utilized as a potent antibacterial agent. Although extensive literature was devoted to proving the antibacterial activity of other metal-based NPs [53], focus on the antibacterial activity of AuNPs/NFs and CuNPs is limited, as such, the present study contributes hugely. MIC was employed to estimate the inhibition AuNPs/NFs, and CuNPs may have on microorganisms. The MICs for the AuNPs and NFs are summarized in Table. Interestingly, the MIC values of the NPs were similar for the bacterial strains. *S. aureus*, *P. aeruginosa* and *B. subtilis* were the most susceptible to AuNFs from all solvents at both 25 °C and 80 °C and showed the lowest viability compared to *K. pneumoniae* and *E. coli*. The authors attributed the activity of the AuNFs to the high-aspect ratio of the elongated petal like surfaces, which induce localised tension and increase reactive oxygen species, thus, causing bacterial membrane rupture [54]. Additionally, the enhancement of *L. discolor* extracts by NPs, improve their ability to disrupt the bacterial cell membrane [54]. The MIC from stem and root extract NPs were similar and exhibited good antibacterial activity against all the bacteria; this may be due to their similar sizes. Contrastingly, all the crude extracts displayed antibacterial activity at only 1000 µg/ml, explaining the significance of the enhancement from nanoparticles.

Table 1. Antibacterial activity of AuNPs, NFs containing *Lannea discolor* extracts.

	AuNFs and NPs (µg/ml)																				
	37	**38**	**39**	**40**	**41**	**42**	**43**	**44**	**45**	**46**	**47**	**48**	**49**	**50**	**51**	**52**	**53**	**54**	**Extracts (µg/ml)**	**G**	**$HAuCl_4$ (1 mM)**
P. aeruginosa	250	125	62,5	62,5	62,5	62,5	62,5	62,5	62,5	125	62,5	7,81	500	500	500	500	1000	1000	1000	7,8	500
K. pneumoniae	250	125	125	250	250	250	250	62,5	125	15,62	15,62	1000	1000	0	0	7,81	62,5	0	1000	7,8	500
E. coli	250	125	1000	500	125	62,5	15,62	15,62	125	125	125	500	500	500	500	31,25	31,25	0	1000	7,8	500
B. subtilis	250	31,25	31,25	31,25	31,25	31,25	31,25	31,25	15,62	62,5	62,5	62,5	62,5	62,5	15,62	15,62	7,81	0	1000	7,8	1000
S. aureus	62,5	62,5	0	62,5	62,5	0	15,62	62,5	125	250	250	500	500	250	500	250	250	0	1000	7,8	1000

Sample keys: 37=Au_ML_25°C; 38 = Au_MS_25°C; 39 =Au_MR_25°C; 40 =Au_ML_80°C; 41=Au_MS_80°C; 42 = Au_MR_80°C; 43 = Au_AL_25°C; 44 = Au_AS_25°C; 45 = Au_AR_25°C; 46 = Au_AL_80°C; 47 =Au_AS_80°C; 48 = Au_AR_80°C; 49 = Au_WL_25°C; 50 =Au_WS_25°C; 51 = Au_WR_25°C; 52 = Au_WL_80°C; 53 = Au_WS_80°C; 54 = Au_WR_80°C; G = Gentamicin ; HAuCl4 = Gold(III) chloride hydrate.

Reports show that the antibacterial activity of AuNPs is associated with their surface modifications, such as shape and the molecules involved in capping the NPs during synthesis [54]. Some bacterial strains, like *S. aureus,* are considered threatful to humans, hence introducing AuNPs as antibacterial agents is fundamental. Morphological interactions, depend on surface orientations for the enhancement of antibacterial activity [55]. NPs with edges rupture the membrane of bacteria and disrupt them. Many experiments on nanoscale surfaces have observed the morphological interactions of AuNPs/NFs with bacteria, confirming the significance of surface orientation for activity [55,56]. In the present study, the high activity can be attributed to the large surface area and

disruptive ability of AuNPs/NFs. Studies have also ascribed the high activity of gold NPs against Gram (-) bacteria to the thin peptidoglycan membrane, and that lower activity is usually observed in gram (+) bacteria with a peptidoglycan membrane with thickness that is 50% higher [57]. However, it is not the case in this study, as activity varies equitably well within both the gram (-) and gram (+) bacteria. Similarly, a few other studies have observed impressive antibacterial activity from AuNPs in both gram (-) and gram (+) bacteria [58-60]. The total MIC for different extracts resembling that of AuCl4 confirms that the activity of phytochemicals improves when incorporated into different nano formulations. The outcome displays that the AuNPs/NFs synthesized from *Lannea discolor* can inhibit the growth of the tested bacteria even at low concentration. The CuNPs in this work showed no activity against tested bacteria, which is ideally indicated by a change in color after addition of Resazurin. This is attributed to the sintered NPs that were unable to interact with the bacterial cells as they are more of a solid mass instead of polydispersed. Other causes may include size, shape, the specific surface area, and surface curvature of the nanoparticles [61]. However, CuNPs in other studies have showed comparable activity in contrast to its counterparts [62]. Possibly, a higher concentration of precursor salts, longer incubation period, may produce CuNPs with better antibacterial activity. Taken together, all these data reported here support the use of the *L discolor* extracts as an alternative to toxic chemical reductants in the production of AuNPs and NFs and CuNPs that can inhibit the growth of different bacteria.

3. Materials and methods

3.1. Collection of plant material

Lannea discolor material was collected from Vuwani (Vhembe district) (23°09'42.9"S 30°25'22.6"E) in the month of November 2018. The plant species were identified by UR with the aid of the literature, and online herbariums (https://plants.jstor.org/compilation; https://powo.science.kew.org) and voucher specimens (UR 01), were prepared and deposited at the University of Venda Herbarium (UVH) in South Africa. *Lannea discolor* material reserved for experiments was air-dried, ground with a pestle and mortar and stored for further use.

3.1.1. Extraction

The air-dried material was ground into a fine powder using a grinding mill (NETZSCH, Selb, Germany). The extracts were obtained by maceration for three 3-day periods at a ratio of 1:10 for solvents, methanol, acetone, and water. They were filtered using filter paper (Whatman No. 1), evaporated to dryness, and stored at 4 °C for subsequent tests.

3.2. Synthesis of nanoparticles

Synthesis of AuNPs and CuNPs was carried using *Lannea discolor* (10mg/ml) extracts. After dissolving 250 mg of gold precursor in 50 mL of distilled water, a stock solution of Gold (III) chloride hydrate (HAuCl4 · aq) that had a concentration of 14 mM. (Millipore, Merck) was prepared. After, the stock solution was diluted to a concentration of 1 mM HAuCl4. The addition of 10 mL of *Lannea discolor* extract to a mixture containing 40 mL of 1 mM HAuCl4 solution was incubated at 25 °C and 80 °C for an hour then in the dark for twenty-four hours. The hue of the solution changed, indicating AuNPs formation. The mixture was centrifuged for ten minutes at 10,000 rpm after being washed twice with distilled water. AuNPs pellets were gathered, air dried, and kept at 4 °C.

To synthesise CuNPs, 1 mM copper (II) sulphate (CuSO4) was made in distilled water, after which, 10 mL of *L discolor* extracts was added to 40 mL copper sulphate solution (1 mM) and incubated at 25 °C and 80 °C for 1 hour. The color of the mixtures changed, indicating formation of CuNPs. After 24 hrs, the nanoparticles were rinsed twice with distillation water, and centrifuged at a speed of 12,000 rpm for 15 min. CuNPs pellets, were dried at 60 °C overnight, then stored at 4 °C for future use.

3.3. Characterisation

 doi:10.20944/preprints202312.0090.v1

3.3.1. Physicochemical Characterization of AuNPs and CuNPs

UV–Vis Spectroscopy Analysis recorded the absorbance of AuNPs and CuNPs in 96 well plates containing 160 µl of NPs using a SpectraMax M3 spectrophotometer (Molecular Devices, California, USA) at wavelengths of 200–800 nm and scan speed of 200 nm/min.

3.3.2. Scanning electron microscopy analysis and energy dispersive x-ray microanalysis

The AuNPs and CuNPs were sonicated for 20 min, after which about 40 µL of each sample was mounted on a glass coverslip attached to a brass stub with adhesive carbon tape and dried under a mercury lamp for about 60 min. The NPs were made conductive with a layer of gold (ca.25mm) using an automated Quorum (Q15OR ES) Module sputter coater (vacuum of 0.1 Torr for 2.5 min) and examined at varying magnification, using a Zeiss Ultra-Plus FEG-SEM at an acceleration voltage of 5 kV. The images were captured with a NIS-D image software, while elemental analysis was done with an energy dispersive X-ray spectrometer (EDX) coupled to an Astronomical Thermal Emission Camera (Aztec) version 1.2 at 20 kV.

3.3.3. Transmission Electron Microscopy analysis and Measurements of Zeta Potential

Carbon coated 200 mesh copper grids were used to scoop a portion of the AuNPs and CuNPs, and dried under a mercury lamp for about 30 min before analysis. The morphology and size of the nanoparticles were determined using a JEOL JEM-2100 TEM at an acceleration voltage of 200 kV.

Zeta analysis was used to measure the surface charge of the NPs using a Zetasizer Nano-Zs90 (Malvern International Ltd, MPT-Z, UK). For each sample, the mean diameter ± SD for ten runs was calculated by applying a multimodal animation.

3.3.4. Fourier Transform Infrared Spectroscopy (FT-IR) Analysis

The ATR-IR FTIR (Alpha 1; Bruker, Germany, Europe) was used to describe the chemically possible compound interactions. The samples were developed and evaluated at a scan range of 4000–400 cm−1. Interpretation of the spectra was achieved by comparing the spectral data with references from identification of functional groups existing in literature [63].

3.4. Antibacterial Assay

The antibacterial activity of the NPs, gentamicin, crude extracts, $HAuCl_4$ and $CuSO_4$ solutions were studied against *Staphylococcus aureus* and *Escherichia coli*, *Pseudomonas aeruginosa*, *Klebsiella pneumoniae* and *Bacillus subtilis* using the minimum inhibitory concentration assay (MIC). A 96 well microtiter plate (Tarsons, Kolkata, India) was prepared by transferring 100 µL of Mueller–Hinton broth under laminar air flow chamber. A volume of 100 µL of NPs, extract and gentamicin was added into the first row of the plate, followed by 10 µL of bacterial inoculum. After which, serial dilutions with concentration 1000 – 7.8 µg/ mL, were performed, and the plates were placed for 24 hrs at 37 °C for incubation. Upon removal, 10 µL of Resazurin solution as per Madikizela *et al* was added to each well followed by further 30 min incubation to determine the MIC value by the observed color change [64].

4. Conclusions

In the current study, a straightforward AuNPs NFs and CuNPs production was reported for the first time employing *Lannea discolor* leaves, stem and roots extracts in a more cost-effective, green technique. The ability of the functional groups in the phytochemicals of *L discolor* to function as a reducing and capping agent is linked to the formation of AuNFs and NPs as well as spherical CuNPs. TEM micrographs provided evidence towards the morphology of AuNPs with several shapes including flowers, spherical, triangular, and hexagonal. The sintered CuNPs can potentially find a unique position in many technological applications such as sensors, flexible devices, and conductivity due to their merged surface area. Despite AuNPs and NFs bacterial activity, more study into their

intricate cytotoxicity profiles is still required. On the other hand, there may be a need to optimise techniques to produce AuNFs and sintered CuNPs from *L discolor*.

Author Contributions: Conceptualization, U.R. and N.A.M.; methodology, U.R. and N.A.A.; formal analysis, U.R.; investigation, U.R.; data curation, U.R.; writing—original draft preparation, U.R. and N.A.M.; writing—review and editing, U.R and N.A.M.; validation, N.A.M.; visualization, U.R and N.A.A.; project administration, N.A.M.; Supervision, N.A.M and A.S; Resources, N.A.M and A.S. All authors have read and agreed to the published version of the manuscript.

Funding: This work was supported by the National Research Foundation (Grant: UID 112386).

Data Availability Statement: The data that support this study will be shared upon reasonable request to the corresponding author.

Acknowledgements: The authors would like to thank by the Faculty of Science Engineering and Agriculture, University of Venda, South Africa for providing the resources needed to conduct the research and the University of KwaZulu Natal Westville Campus Microscopy and Microanalysis unit for facilities.

Conflicts of Interest: The authors declare no conflicts of interest.

References

1. Malike, S.; Muhammad, K.; Waheed, Y. Nanotechnology: A revolution in modern industry. *Molecules.* **2023**, *28*, 661.
2. Khan, I.; Saeed, K.; Khan, I. Nanoparticles: Properties, applications, and toxicities. *Arab. J. Chem.* **2019,** *12,* 908-931.
3. Szczyglewska, P.; Feliczak-Guzik, A.; Nowak, I. Nanotechnology–General Aspects: A Chemical Reduction Approach to the Synthesis of Nanoparticles. *Molecules.* **2023**, *28*, 4932
4. Singh. J.; Dutta, T.; Kim, K.H.; Rawat, M.; Samddar, P.; Kumar, P. Green synthesis of metals and their oxide nanoparticles: applications for environmental remediation. *J. Nanobiotechnology.* **2018,** *16* ,1-24.
5. Egorova, K.S.; Ananikov, V.P. Which metals are green for catalysis? Comparison of the toxicities of Ni, Cu, Fe, Pd, Pt, Rh, and Au salts. *Angew. Chem. Int. Ed.* **2016,** *55*, 12150-12162.
6. Louis, C.; Pluchery, O. Gold nanoparticles in the past: before the nanotechnology era gold nanoparticles for physics, chemistry, and biology (Singapore: World Scientific Publishing). **2012,** p 1-28.
7. Chiang, M.C.; Nicol, C. J.; Lin, C. H.; Chen, S.J.; Yen, C.; Huang, R. N. Nanogold induces anti-inflammation against oxidative stress induced in human neural stem cells exposed to amyloid-beta peptide. *Neurochem. Int.* **2021,** *145*, 104992
8. Leary, J. Attaching Biomolecules to Nanoparticles (Cambridge: Cambridge University Press). **2022**, p 103-121.
9. Kulkarni, D.; Sherkar, R.; Shirsathe, C.; Sonwane, R.; Varpe, N.; Shelke, S.; More, M.P.; Pardeshi, S.R.; Dhaneshwar, G.; Junnuthula, V.; Dyawanapelly, S. Biofabrication of nanoparticles: sources, synthesis, and biomedical applications. *Front. bioeng. biotechnol.* **2023**, *11*, 1159193.
10. Sheny, D.S.; Joseph, M.; Daizy, P. Phytosynthesis of Au, Ag and Au-Ag bimetallic nanoparticles using aqueous extract and dried leaf of *Anacardium occidentale. Spectrochim. Acta A.* **2011**, *79*, 254.
11. Pechyen, C.; Ponsanti, K.; Tangnorawich, B.; Ngernyuang, N. Biogenic synthesis of gold nanoparticles mediated by *Spondias dulcis* (Anacardiaceae) peel extract and its cytotoxic activity in human breast cancer cell. *Toxicol. Rep.* 2022, 9, 1092.
12. Alhumaydhi, F.A. Green synthesis of gold nanoparticles using extract of *Pistacia chinensis* and their *in vitro* and *in vivo* biological activities. *J. Nanomater.* **2022**, *1*, 11.
13. Crisan, M.C.; Teodora, M.; Lucian, M. Copper nanoparticles: Synthesis and characterization, physiology, toxicity, and antimicrobial applications. *Appl. Sci.* **2021**, *12*, 141.
14. Athanassiou, E.K.; Grass, R.N.; Stark, W.J. Large-scale production of carbon-coated copper nanoparticles for sensor applications. *Nanotechnology*. **2006**, *17,* 1668.
15. Zhou, Q.; Zhou, M.; Li, Q.; Wang, R.; Fu, Y.; Jiao, T. Facile biosynthesis and grown mechanism of gold nanoparticles in *Pueraria lobata* extract. *Colloids Surf. A: Physicochem. Eng.* **2019**, 567, 69.
16. Martínez-Vieyra, C.; Olguin, M.T.; Gutiérrez-Segura, E.; López-Tellez, G. Comparison of Ag, Cu and Zn nanoparticles obtained using *Aloe vera* extract and gamma ionizing radiation. *J. Appl. Res. Technol.* **2020**, 18, 289-314.
17. Wu, S.; Rajeshkumar, S.; Madasamy, M.; Mahendran, V. Green synthesis of copper nanoparticles using *Cissus vitiginea* and its antioxidant and antibacterial activity against urinary tract infection pathogens. *Artif. Cells. Nanomed. Biotechnol.* **2020**, *48,* 1153.

18. Varghese, B.; Kurian, M.; Krishna, S.; Athira, T.S. Biochemical synthesis of copper nanoparticles using *Zingiber officinalis* and *Curcuma longa*: Characterization and antibacterial activity study. *Mater. Today: Proc.* **2020**, *25*, 302.
19. Sundaram, C.S.; Kumar, J.S.; Kumar, S.S.; Ramesh, P.L.N.; Zin, T.; Rao, U.M. 2020 Antibacterial and anticancer potential of *Brassica oleracea var acephala* using biosynthesised copper nanoparticles. *Med. J. Malaysia*. **2020**, *75*, 677.
20. Shubhashree, K.R.; Reddy, R.; Gangula, A.K.; Nagananda, G.S.; Badiya, P.K.; Ramamurthy, S.S.; Reddy, N. Green synthesis of copper nanoparticles using aqueous extracts from *Hyptis suaveolens* (L). *Mater. Chem. Phys.* **2022**, *280*, 125795.
21. Maroyi, A. *Lannea discolor*: its botany, ethnomedicinal uses, phytochemistry, and pharmacological properties. *Asian. J. Pharm. Clin. Res.* **2018**, *11*, 49.
22. Mwamatope, B.; Tembo, D.; Kampira, E.; Maliwichi-Nyirenda, C.; Ndolo, V. Seasonal variation of phytochemicals in four selected medicinal plants. *Pharmacognosy. Res.* **2021**, *13*, 218.
23. Abdallah, B.M.; Ali, E.M. Therapeutic Potential of Green Synthesized Gold Nanoparticles Using Extract of *Leptadenia hastata* against Invasive Pulmonary Aspergillosis. *J. Fungi*. **2022**, *8*, 442.
24. Liu, K.; He, Z.; Curtin, J.F.; Byrne, H.J.; Tian, F. A novel, rapid, seedless, in situ synthesis method of shape and size controllable gold nanoparticles using phosphates. *Sci. Rep*. **2019**, *9*, 7421.
25. Liebig, F.; Henning, R.; Sarhan, R.M.; Prietzel, C.; Bargheer, M.; Koetz, J. A new route to gold nanoflowers. *Nanotechnology*. **2018**, *29*, 185603.
26. Gao, L.; Mei, S.; Ma, H.; Chen, X. Ultrasound-assisted green synthesis of gold nanoparticles using citrus peel extract and their enhanced anti-inflammatory activity. *Ultrason. Sonochem.* **2022**, *83*, 105940.
27. Mthembu, S.B.; Akintayo, D.C.; Moodley, B.; Gumbi, B.P. Development of gold plasmonic nanoparticles for detection of polydiallyldimethylammonium chloride at Umgeni water treatment plants: An optimised study and case application. *Heliyon*. **2023**, *9*, e17136.
28. Das, P.E.; Abu-Yousef, I.A.; Majdalawieh, A.F.; Narasimhan, S.; Poltronieri, P. Green synthesis of encapsulated copper nanoparticles using a hydroalcoholic extract of *Moringa oleifera* leaves and assessment of their antioxidant and antimicrobial activities. *Molecules.* **2022**, *25*, 555.
29. Kim, H.S.; Lee, D.Y.Near-infrared-responsive cancer photothermal and photodynamic therapy using gold nanoparticles. *Polym.* **2018**, *10*, 961.
30. Amjad, R.; Mubeen, B.; Ali, S.S.; Imam, S.S.; Alshehri, S.; Ghoneim, M.M.; Alzarea, S.I.; Rasool, R.; Ullah, I.; Nadeem, M.S.; Kazmi, I. Green synthesis and characterization of copper nanoparticles using *Fortunella margarita* leaves. *Polym.* **2021**, *13*, 4364.
31. Babalola, B.J.; Ayodele, O.O.; Olubambi, P.A. Sintering of nanocrystalline materials: Sintering parameters. *Heliyon*. **2023**, *9*, e14070.
32. Hong, G.B.; Wang, J.F.; Chuang, K.J.; Cheng, H.Y.; Chang, K.C.; Ma, C.M. Preparing Copper Nanoparticles and Flexible Copper Conductive Sheets. *Nanomater.* **2022**, *12*, 360.
33. Sarwax, N.; Choi, S.H.; Dastgeer, G.; Humayoun, U.B.; Kumar, M; Nawaz, A.; Jeong, D.I.; Zaidi, S.F.; Yoon, D.H. Synthesis of citrate-capped copper nanoparticles: A low temperature sintering approach for the fabrication of oxidation stable flexible conductive film. *Appl. Surf. Sci.* **2021**, 542, 148609.
34. Keskin, C.; Atalar, M.N. Firat Baran, M.; Baran, A. Environmentally friendly rapid synthesis of gold nanoparticles from *Artemisia absinthium* plant extract and application of antimicrobial activities. *JIST.* **2021**, *11*, 365.
35. Ismail, M.; Gul, S.; Khan, M.I.; Khan, M.A.; Asiri, A.M.; Khan, S.B. Green synthesis of zerovalent copper nanoparticles for efficient reduction of toxic azo dyes congo red and methyl orange. *Green Process. Synth.* **2019**, *8*, 135.
36. Sajanlal, P.R.; Sreeprasad, T.S.; Samal, A.K.; Pradeep, T. Anisotropic nanomaterials: structure, growth, assembly, and functions. *Nano. Rev.* **2011**, *2*, 5883.
37. Jakhmola, A.; Vecchione, R.; Gentile, F.; Profeta, M.; Manikas, A.C.; Battista, E.; Netti, P.A. Experimental and theoretical study of biodirected green synthesis of gold nanoflowers. *Mater. Today Chem.* **2019**, *14*, 100203.
38. Ji, Y.; Ren, M.; Li, Y.; Huang, Z.; Shu, M.; Yang, H.; Xiong, Y.; Xu, Y. Detection of aflatoxin B1 with immunochromatographic test strips: enhanced signal sensitivity using gold nanoflowers. *Talanta.* **2015**, *142*, 206.
39. Borah, D.; Hazarika, M.; Tailor, P.; Silva, A.R.; Chetia, B.; Singaravelu, G.; Das, P. Starch-templated biosynthesis of gold nanoflowers for in vitro antimicrobial and anticancer activities. *Appl. Nanosci.* **2018**, *8*, 241.
40. Onmaz, N.E.; Demirezen, Yilmaz, D.; Imre, K.; Morar, A.; Gungor, C.; Yilmaz, S.; Gundog, D.A.; Dishan, A.; Herman, V.; Gungor, G. Green synthesis of gold nanoflowers using *Rosmarinus officinalis* and

Helichrysum italicum extracts: Comparative studies of their antimicrobial and antibiofilm activities. *Antibiotics*. **2022**, *11*, 1466.

41. Deshmukh, A.R.; Kim, B.S. Flower-like biogenic gold nanostructures for improved catalytic reduction of 4-nitrophenol. *J. Environ. Chem. Eng.* **2021**, *9*, 106707.
42. Pluchery, O.; Remita, H.; Schaming, D. Demonstrative experiments about gold nanoparticles and nanofilms: an introduction to nanoscience. *Gold Bull.* **2013**, *46*, 319.
43. Tanaka, R.; Yuhi, T.; Nagatani, N.; Endo, T.; Kerman, K.; Takamura, Y.; Tamiya, E. A novel enhancement assay for immunochromatographic test strips using gold nanoparticles. *Anal. Bioanal. Chem.* **2006**, *385*, 1414.
44. Merza, K.S.; Al-Attabi, H.D.; Abbas, Z.M.; Yusr, H. A Comparative Study on Methods for Preparation of Gold Nanoparticles. *Green. Sustain. Chem.* **2011**, *2*. 26.
45. Kariuki, V.M.; Hoffmeier, J.C.; Yazgan, I.; Sadik O.A. Seedless synthesis and SERS characterization of multi-branched gold nanoflowers using water soluble polymers. *Nanoscale.* **2017**, *9* 8330.
46. Shabestarian, H.; Homayouni-Tabrizi, M.; Soltani, M.; Namvar, F.; Azizi, S.; Mohamad, R.; and Shabestarian H. Green synthesis of gold nanoparticles using *sumac* aqueous extract and their antioxidant activity. *Mater. Res.* **2016**, *20*, 264.
47. Donga, S.; Bhadu, G.R.; Chanda, S. Antimicrobial, antioxidant, and anticancer activities of gold nanoparticles green synthesized using *Mangifera indica* seed aqueous extract. *Artif. Cells. Nanomed. Biotechnol.* **2020**, *48*, 1315.
48. Song, J.Y; Jang, H.K.; Kim, B.S. Biological synthesis of gold nanoparticles using *Magnolia kobus* and *Diopyros kaki* leaf extracts. *Process. Biochem.* **2009**, *44*, 1133.
49. Chopra, H.; Bibi, S.; Singh, I.; Hasan, M.M.; Khan, M.S.; Yousafi, Q.; Baig, AA.; Rahman, M.M.; Islam.; Emran, T.B.; Cavalu, S. Green metallic nanoparticles: biosynthesis to applications. *Front. bioeng. biotechnol.* **2022**, *10*, 548.
50. Patra, J.K.; Das, G.; Fraceto, L.F.; Campos, E.V.; Rodriguez-Torres, M.D.; Acosta-Torres, L.S.; Diaz-Torres, L.A.; Grillo, R.; Swamy, M.K.; Sharma, S.; Habtemariam, S. Nano based drug delivery systems: recent developments and future prospects. *J. Nanobiotechnology*. **2018**, *16*, 1.
51. Gawande, M.B.; Goswami, A.; Felpin, F.X.; Asefa, T.; Huang, X.; Silva, R.; Zou, X.; Zboril, R.; Varma, R.S. Cu and Cu-based nanoparticles: synthesis and applications in catalysis. *Chem. Rev*. **2016,** *116*, 3722-3811.
52. Sizochenko, N.; Mikolajczyk, A.; Syzochenko, M.; Puzyn, T.; Leszczynski, J. Zeta potentials (ζ) of metal oxide nanoparticles: A meta-analysis of experimental data and a predictive neural network modelling. *NanoImpact.* **2021**, *22*, 100317.
53. Murthy, H.C.; Desalegn, T.; Kassa, M.; Abebe, B.; Assefa, T. Synthesis of green copper nanoparticles using medicinal plant *Hagenia abyssinica* (Brace) JF Gmel leaf extract: Antimicrobial properties. *J. Nanomater.* **2020,** *1*, 3924081.
54. Yu, Z.; Li, Q.; Wang, J.; Yu, Y.; Wang, Y.; Zhou, Q.; Li, P. Reactive oxygen species-related nanoparticle toxicity in the biomedical field. *Nanoscale Res. Lett.* **2020**, *15*, 115.
55. Yougbare, S.; Chang, T.K.; Tan, S.H.; Kuo, J.C.; Hsu, P.H.; Su, C.Y.; Kuo, T.R. Antimicrobial gold nanoclusters: Recent developments and future perspectives. *Int. J. Mol. Sci.* **2019**, *20*, 2924.
56. Mousavi, S.M.; Zarei, M.; Hashemi, S.A.; Ramakrishna, S.; Chiang, W.H.; Lai, C.W.; Gholami, A. Gold nanostars-diagnosis, bioimaging and biomedical applications. *Drug Metab. Rev.* **2020**, *52*, 299.
57. Okkeh, M..; Bloise, N.; Restivo, E.; De Vita, L.; Pallavicini, P.; Visai, L. Gold nanoparticles: can they be the next magic bullet for multidrug-resistant bacteria? *Nanomater.* **2021**, *11*, 312.
58. Umadevi, M.; Rani, T.; Balkrishnan, T.; Ramanibai, R. Antimicrobial activity of silver nanoparticles under an ultrasonic field. *Int. J. Pharm. Sci. Nanotechnol.* **2011**, *4*, 1491.
59. Zheng, K.; Setyawati, M.I.; Leong, D.T.; Xie, J. Antimicrobial Gold Nanoclusters. *ACS Nano*. **2017**, *11*, 6904.
60. Rovati, D.; Albini, B.; Galinetto, P.; Grisoli, P.; Bassi, B.; Pallavicini, P.; Dacarro, G.; Taglietti, A. High Stability Thiol-Coated Gold Nanostars Monolayers with Photo-Thermal Antibacterial Activity and Wettability Control. *Nanomater.* **2019**, *9*, 1288.
61. Montes de Oca-Vásquez, G.; Solano-Campos, F.; Vega-Baudrit, J.R.; López-Mondéjar, R.; Odriozola, I.; Vera, A.; Moreno, J.L.; Bastida, F. Environmentally relevant concentrations of silver nanoparticles diminish soil microbial biomass but do not alter enzyme activities or microbial diversity. *J. Hazard. Mater*. **2020**, *391*, 122224.
62. Qamar, H.; Rehman, S.; Chauhan DK, Tiwari, AK;. Upmanyu, V. Green Synthesis, Characterization and Antimicrobial Activity of Copper Oxide Nanomaterial Derived from *Momordica charantia*. *Int J Nanomedicine*. **2020**, *15*, 2541-2553
63. Coates, J. Interpretation of infrared spectra, a practical approach In Encyclopedia of Analytical Chemistry ed, Meyers, R.A.; John Wiley & Sons, Ltd., USA, **2000**; P 10815.

64. Madikizela, B.; Ndhlala, AR.; Finnie, J.F.; Staden, J.V. In vitro antimicrobial activity of extracts from plants used traditionally in South Africa to treat tuberculosis and related symptoms. *Evid. Based Complementary Altern. Med*. **2013**, *1*, 1.